Investigating the therapeutic potential of extracellular vesicles from hiPSCs and hiPSC-derived cardiac cells for heart regeneration

Marta Oliveira

Instituto Superior Técnico, December 2020

Abstract

Recent years have seen a shift from cell-based to cell-free therapeutic strategies in the cardiovascular field, given the new found role of the cellular secretome, including extracellular vesicles (EVs), in the processes that regulate cardiac repair and regeneration. In this work, EVs from hiPSCs and hiPSC-derived cardiac cells were isolated and purified from conditioned culture medium by differential centrifugation and density gradient ultracentrifugation. *In vitro* bioactivity assays were used to assess wound healing and angiogenic properties of EV samples. hiPSC-EVs demonstrated more significant wound healing capacity and the ability to stimulate the formation of capillary-like structures when used as treatment in endothelial cells, when compared to EVs from cardiac-derived groups. MicroRNA expression profiles obtained by RNA-seq indicated specificity of EV cargo, substantiated by the enrichment of cardiac-derived EVs in microRNAs involved in cardiac muscle development. hiPSC-EVs displayed increased targeting of pro-survival and angiogenesis-related pathways. Additional work will be paramount to validate and enhance the bioactivity of cardiac-derived EVs and to further unveil the role of hiPSC-EVs in cardioprotection.
Keywords: extracellular vesicles, human induced pluripotent stem cells, cardiomyocyte differentiation, angiogenesis, cardiac regenerative medicine

Introduction

Cardiovascular disease is the dominant cause of morbidity and mortality worldwide (1), with current therapies still failing to address the fundamental mechanisms of cardiac tissue regeneration. Cell transplantation strategies have failed to demonstrate clinically meaningful results, showing inconsistent and modest efficacy (2). Recently, it has become increasingly apparent that the therapeutic effects of transplanted cells are largely mediated by secreted factors that stimulate endogenous repair. Mounting evidence suggests extracellular vesicles (EVs) to be among these paracrine mediators, playing a major role in cardiac rehabilitation processes (3; 4).

EVs are nano- and micro-sized particles delimited by a lipid bilayer and without a functional nucleus that transport a cargo of biomolecules between cells, including proteins, nucleotides, lipids and metabolites (5). They are naturally released during normal cellular physiology, as well as during stress and disease (6), acting as facilitators in intercellular communication. In eukaryotic cells, EVs are secreted either by fusion of endosomal compartments with the plasma membrane, shedding of the plasma membrane, or during controlled cell death. Thus, the nomenclature of EV is generally associated with their origin and size, being described as exosomes (50-150nm), microvesicles (100-1000nm) or apoptotic bodies (500nm-5µm) accordingly (7).

In cardiac regenerative medicine, there is a growing interest in using EVs as cell-mimetic therapeutics, given their potential superior benefits (8) and also their advantages over cell transplantation, such as absence of oncologic risk and feasibility of consistent large-scale production (9). Recently, EVs were shown to be virtually non-immunogenic (10), crossing an important prerequisite for clinical translation. Research has focused on the cardioprotective potential of EVs derived from adult (stem) cells, with more limited avaliability, such as mesenchymal stem/stromal cells (MSCs) (11) and cardiac progenitor cells (CPCs) (12; 13), along with a more recent focus on cardiomyocytes (CMs) (14). The use of human induced pluripotent stem cell (hiPSC) derivatives as cell sources for EV production presents advantages over alternative adult cells given their high self-renewal and proliferation properties, however few comparative studies have been conducted to define the most promising cell candidates within hiPSC-derivatives.

In this work, EVs were isolated from conditioned culture medium of four well-defined cell populations: hiPSCs, hiPSC-CPCs, immature (CMi) and mature (CMm) hiPSC-CMs. Particle characteris-

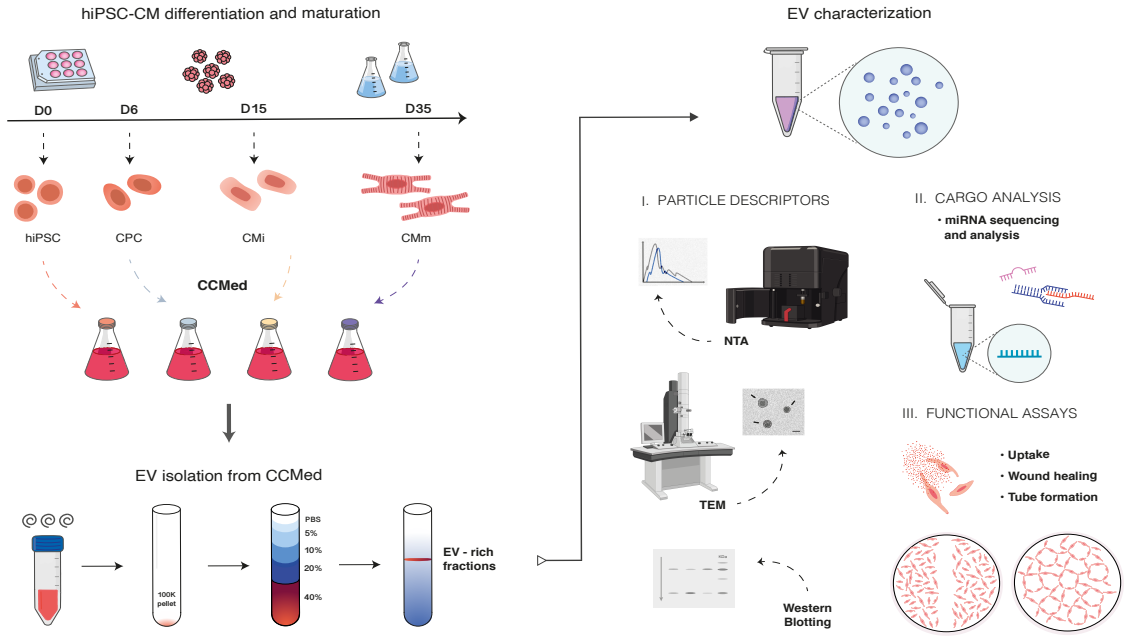

Figure 1: Overview of the experimental workflow for cardiomyocyte differentiation and EV isolation from different cell populations: human induced pluripotent stem cells (hiPSCs) and their derivatives including, cardiac progenitor cells (CPCs), immature and mature cardiomyocytes (CMi and CMm). hiPSCs were differentiated into CMs using a 3D differentiation protocol previously developed by iBET. Conditioned culture medium (CCMed) was harvested at days 0 (hiPSCs), 6 (CPCs), 15 (CMi) and 35 (CMm) of culture and processed by multiple centrifugation steps and 0.45 µm filtration to remove major contaminants. The cleared CCMed was ultracentrifuged at 110.000 g_{max} for 2h40 min to produce a 100K pellet, which was loaded on the bottom of an OptiPrep™ density gradient and centrifuged for 18h at 110.000 g_{max}. EV-rich density fractions 8-9 were collected and concentrated. Particle characterization was performed to ensure purity of EV samples, and functional assays were carried out to assess therapeutic potential of EVs in the cardiac setting. MicroRNA analysis was perfomed to give further insights on target functions and specificity of released EV cargo.

tics, function and microRNA cargo were compared with the goal of studying their therapeutic potential and further understand how EV function is influenced by the differentiation and maturation state of their parent cell. This work may open new directions on the design of novel cell-free therapeutic approaches for heart regenerative medicine.

Results & Discussion

Establishment of an effective EV isolation and purification method and EV characterization

The choice of isolation method is a critical parameter known to significantly impact size, yield and purity of EV samples (15). OptiPrep™ density gradient, the adopted method for this work (Fig.1), has been shown to outperform other commonly used approaches in terms of enrichment in exosomal markers and absence of contaminants by several independent studies (16; 17; 18).

The isolation protocol was validated by standard particle characterization. For this, NTA was performed on EV samples to assess size distribution and particle concentration. Results indicated a typical NTA profile for the size distribution of all samples, ranging between 50 and 500 nm (Fig.2a). More specifically, particle concentration peaks occur for particle sizes of 134.5 and 176.5 nm for hiPSC-EVS, 138.5 nm for CPC-EVs, 105.5 nm and 139.5 nm for CMi-EVs and 127.5 nm for CMm-EVs, which stand within the reported range for EV size (30-1000 nm) (7).

The yield of EVs was estimated to appropriately compare the EV production capacity of each cell type, defined as the total number of isolated particles secreted per million viable cells per day of production (Fig.2b). When considering the number of cells in culture, EV yield analysis indicates a distinct profile regarding EV production capacity to that which might be interpreted following NTA results. Contrary to previous findings that reported limited EV release by CMs relative to CPCs (19), when normalization to the number of EV-producing cells is performed, CPCs seem to give the lowest EV yield (8.50×10^6 particle.10^6 cell^{-1}.day^{-1}), in spite of showing the greatest particle concentration by NTA. Furthermore, EV yield is highly influenced by the choice of isolation method (20). Given that the present methodology contains an exhaustive series of centrifugation steps, it may compromise yield to a similar extent in all samples.

Visualization of particles by Transmission Electron Microscopy (TEM) showed typical EV morphology and absence of similar-sized contaminant particles such as low-density lipoproteins (LDLs)

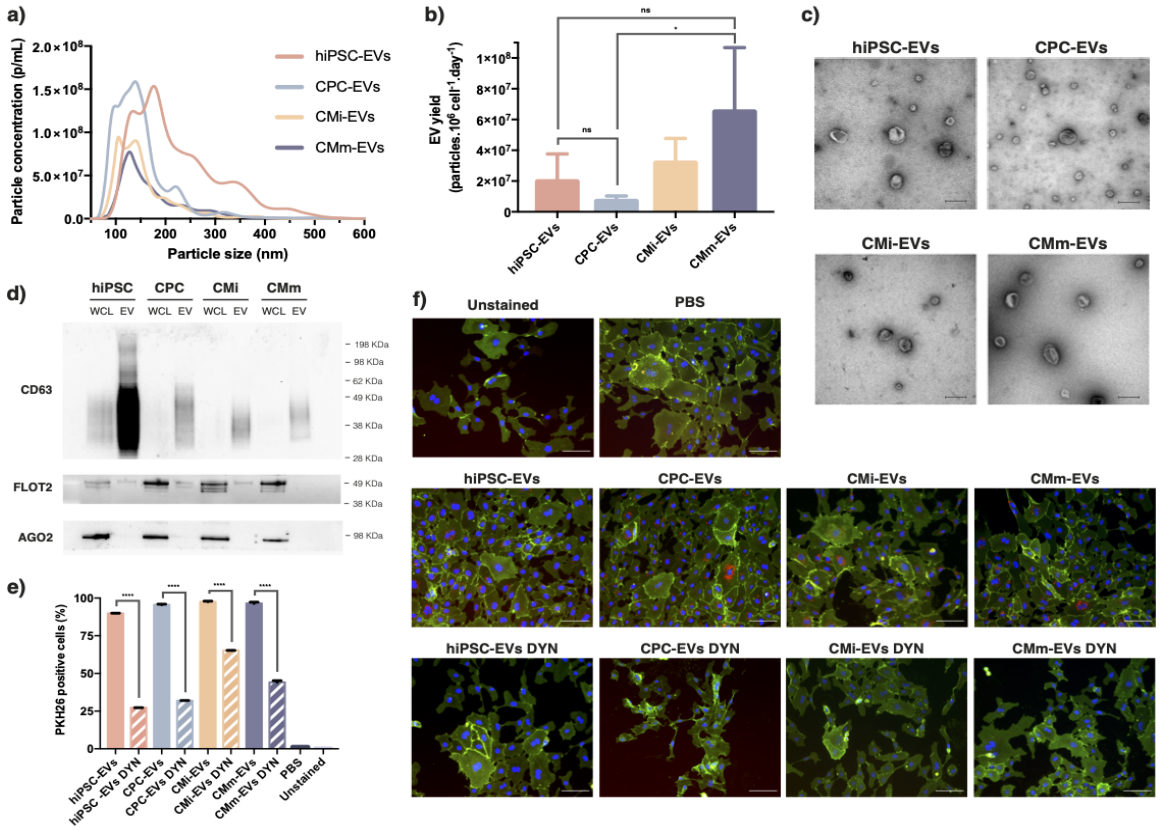

Figure 2: Characterization of EV samples and uptake of PKH26-labelled EVs by HUVECs. a) Size distribution profile of EV samples as analysed by Nanoparticle Tracking Analysis, expressed in particles per mL of sample (n=4). **b)** EV yield, measured as total number of isolated particles per million viable cells per day ($n \geq 3$ for all samples). **c)** Representative negative staining close-field transmission electron microscopy (TEM) images of EV samples. Scale bar: 200 µm **d)** Western blot analysis of characteristic EV markers (transmembrane protein CD63 and cytosolic protein Flotillin-2) and co-isolated contaminant (Argonaute 2) of EV samples and respective cell lysate. WCL – whole cell lysate. **e)** Percentage of PKH26-positive cells quantified by flow cytometry. **f)** Representative immunofluorescence images of EV uptake and uptake blockage. HUVECs incorporated PKH26-labelled EVs, as seen by the red dots present inside the cells. EV uptake was blocked by the presence of Dynasore (DYN). HUVECs were stained for transmembrane protein CD31 (green) and nuclei were counterstained with DAPI (blue). Scale bar: 100 µm. Results shown as mean ± SD. * $p < 0.1$, **** $p < 0.0001$, ns non-significant.

(Fig.2c). Western Blot analysis further confirmed the identity of isolated samples by the detection of EV-specific markers CD63 and Flotillin 2, and absence of non-EV contaminant Argonaute 2 (Fig.2d) (21).

HUVECs were incubated with labelled EVs to study cellular uptake (Fig.2 e-f). From the resulting immunofluorescence images, EVs can be detected in the cell cytoplasm by the visible red fluorescent signal. Uptake blockage was performed using Dynasore, a GTPase inhibitor which acts on Dynamin-2 to prevent detachment of the endocytic vesicle from the cell membrane during clathrin- and caveolae-dependent endocytosis, inhibiting EV internalization by recipient cells. For a quantitative analysis of EV internalization, flow cytometry was performed to assess the percentage of PKH26-positive cells after treatment with labelled vesicles. Results show no major differences in the number of cells with fluorescent signal, which equates to a near total cell population for all EV samples. Interestingly, in the presence of Dynasore, the percentage of PKH26-positive cells is lower but not null compared to the non-DYN counterparts. This indicates that while most EVs are uptaken by HUVECs via dynamin-dependent processes, a subpopulation of EVs continues to be internalized via alternative dynamin-independent pathways upon dynamin inhibition.

Wound healing and angiogenic properties of EVs

Angiogenesis, the intricate process by which new blood vessels are formed from pre-existing ones, is a fundamental step for cardiac tissue rehabilitation following assault (22). Angiogenesis is mediated by migration, proliferation and remodelling of endothelial cells following complex molecular signalling mechanisms and cellular crosstalk (22). To study the involvement of EVs in the collective migration and tube formation capacities of endothelial cells, two functional assays were performed on HUVECs.

Results demonstrate that all EV samples exhibit

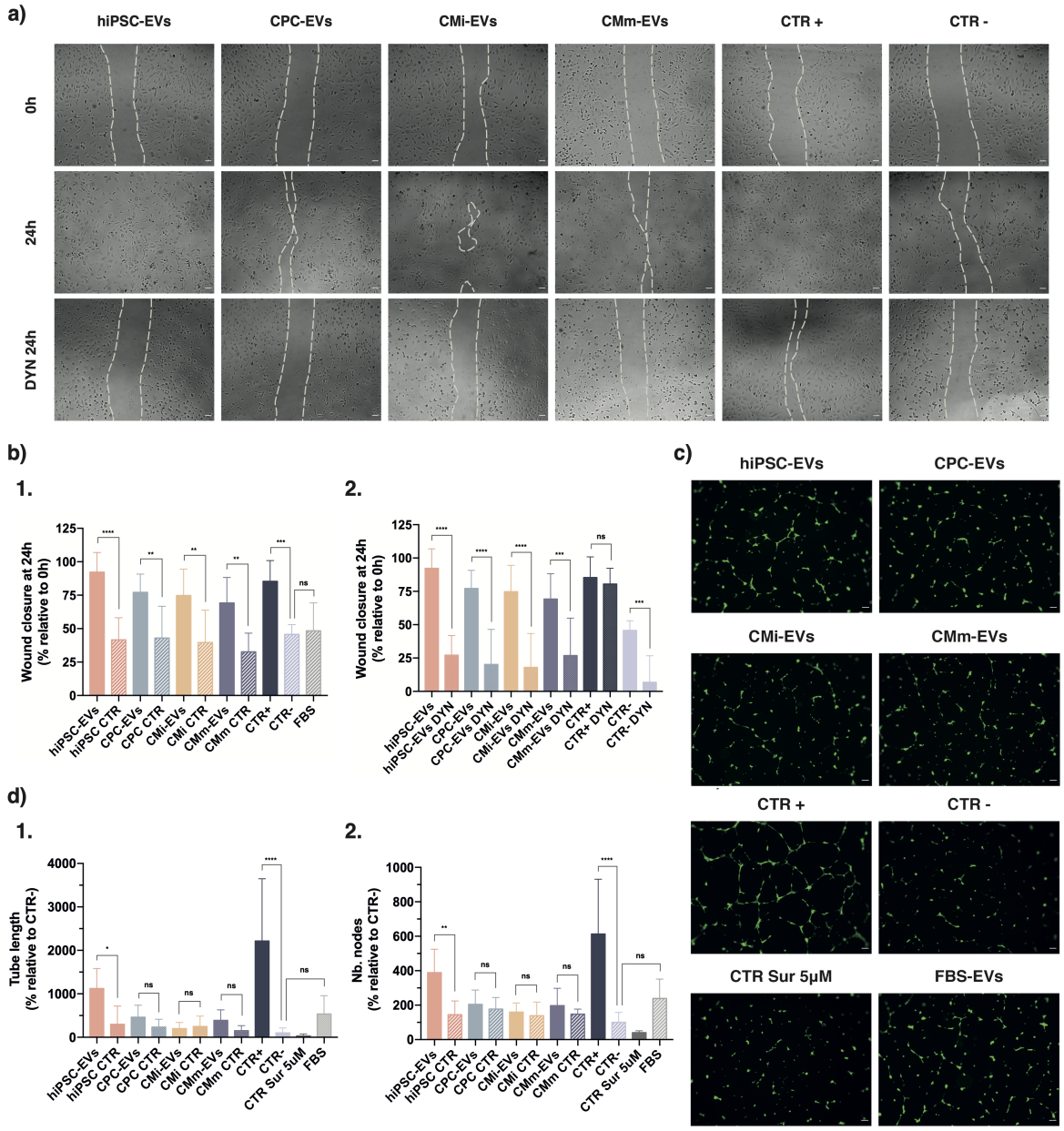

Figure 3: Effect of EVs from hiPSCs and hiPSC-cardiac derivatives on HUVEC migration and angiogenesis, quantified by the wound healing and tube formation assays a) Representative images of cell migration at timepoints 0h and 24h post-scratch, in absence or presence of Dynasore. Scale bar: 100 µm. **b)** Percentage of wound closure at 24h relative to wound area at 0h, with the respective comparison to **1.** negative or vehicle control, and **2.** treatment in the presence of Dynasore. **c)** Representative images of tube formation at timepoint 8h post-seeding. Scale bar: 100 µm. **c)** Quantification of tube formation as percentage of **1.** tube length and **2.** number of nodes, relative to untreated control (CTR-, corresponding to 100%). All data shown as mean ± SD (n=3). *p $<$ 0.1, **p $<$ 0.01, ***p $<$ 0.001, ****p $<$ 0.0001, ns non-significant.

significant capacities to promote HUVEC migration (Fig.3 a-b). This migratory stimulation is observed to a similar extent for all groups, with enhanced significance for hiPSC-EVs. Furthermore, this effect is suppressed with the addition of Dynasore, suggesting that the observed outcome is impacted by EV activity. The following experimental outcome goes in accordance with previously reported studies on EC migration that verify the wound healing effects of CPC- and CM-EVs (14; 23), possibly due to the matrix degradation and remodelling action of matrix metalloproteinases (MMPs) found in secreted vesicles. In addition, the inability of FBS-EVs to close the wound could advocate for specificity in EV activity.

The same was not observed for the tube formation assay, given that only hiPSC-EVs displayed significant capacity to induce formation of capillary-like structures in HUVECs (Fig.3 c-d). The remaining EV samples showed no angiogenic properties from both analysed measurements when compared to their vehicle controls, and in similar

degree to that of FBS-EVs. These findings oppose those reported in the literature by several independent groups, that indicate pro-angiogenic activity for CPC-EVs (13; 19) and CMs (14; 24), along with the established therapeutic properties found for hiPSC-EVs (25). Furthermore, it would be expected that cardiac-derived EVs would be equally or more effective at stimulating cardiac repair mechanisms than EVs from unrelated cell sources (26).

Still, it is important to consider that the present analysis does not account for a number of factors which may play a role in the experimental outcome. Firstly, the functional assays adopted for this work are purely observational and may not represent the most suitable models for the study of the cardiotherapeutic potential of EVs. Additionally, it is not certain that the same number of particles is being uptaken by HUVECs for each different sample, nor that their cargo is being internalized uniformly.

MicroRNA profile of EV cargo

To better interpret the results obtained from functional assays and gain insight into the specific signals directed to the cells, transcriptomic analysis of EV cargo was performed.

Differential Expression (DE) data for each group comparison indicates distinct microRNA expression profiles for EVs from different cell groups (Fig.4a). Interestingly, the further apart these cell sources stand in the differentiation and maturation timeline, the more their respective EV microRNA profiles diverge (Fig.4a-1), also seen by the increasing number of differentially expressed miRNAs from hiPSC-EVs when compared to CPC, CMi and CMm-EVs (Fig.4a-2). This suggests specificity of EV cargo and specialized stimuli for each destined target according to its cell source, a finding that has been previously reported (27). These results are supported by the Principal Component Analysis (PCA) (Fig. 4b), which shows two major clusters for EVs from hiPSCs (blue) and cardiac derivative cells (red) along Principal Component 1 (PC1). Furthermore, specific differentially expressed miRNAs involved in cardiac muscle development and maturation (28; 29) were found to be highly overexpressed in CPC/CMi/CMm-EVs (Fig. 4c).

Figure 4 d) shows the results obtained for KEGG pathway analysis of miRNA targets. For every KEGG class, each containing a set of related pathways, the number of targeted genes is shown for CPC/CMi/CMm-EVs (purple) and hiPSC-EVs (orange). KEGG analysis results show that Cellular Processes implicated in wound healing and angiogenesis are significantly enriched in hiPSC-EVs. These include cell motility and community processes, such as regulation of the actin cytoskeleton, junctional proteins and focal adhesion, all key activities for vascular angiogenic response (30). Additionally, hiPSC-EVs show increased targeting of signalling pathways regulating pluripotency of stem cells, advocating for EV specificity.

Gene Ontology (GO) enrichment analysis yielded an extensive array of biological processes associated with targeted genes (Fig.4e). Biological processes contained within the categories of circulatory system development, response to wounding and cellular component organization were identified for hiPSC-EVs and CPC/CMi/CMm-EVs groups. Results suggest enrichment of relevant biological functions, such as blood coagulation, platelet activation, growth factor signalling and cytoskeleton/extracellular matrix organization in hiPSC-EVs, all considered important modulators of angiogenesis and vessel integrity (31; 32). Furthermore, overexpression of reported pro-angiogenic miRNAs was detected in hiPSC-EVs, including miR-18a, miR-20a and miR-17-5 of the miR-17-92 cluster. Such findings, although not conclusive, could attest to the more pronounced angiogenic effects observed for hiPSC-EVs. However, from a first set of results, no evident trace stands out to firmly substantiate the outcome of functional assays. A more in-depth analysis and subsequent experimental confirmation by miRNA inhibition/overexpression would be required to reach conclusions regarding the potential role of EVs in cardioprotection and the most promising parent cells for this purpose.

Conclusions and future work

In this work, we established a method for the isolation of pure EVs from CCMed of hiPSC and hiPSC-derived CPC, CMi and CMm cells by density gradient ultracentrifugation. While all four EV populations were promigratory, only hiPSC-EVs demonstrated the capacity to promote tube formation in HUVECs, an observation that may be explained by more significant expression of pro-angiogenic and cardioprotective microRNAs in the transcriptomic cargo of this EV population. More extensive data analysis and experimental confirmation will be required to reach conclusive results.

These results suggest hiPSC-EVs as a suitable candidate for therapeutic use in cardiac repair, although its beneficial effects were not pronounced when compared to the remaining cardiac-derived EV groups. Strategies involving cell preconditioning for the modulation of EV signalling towards a more specific cardioprotective response have been employed in numerous studies (14; 33; 34) and reveal promising results for boosting the therapeutic potential of EV treatment. Similar approaches

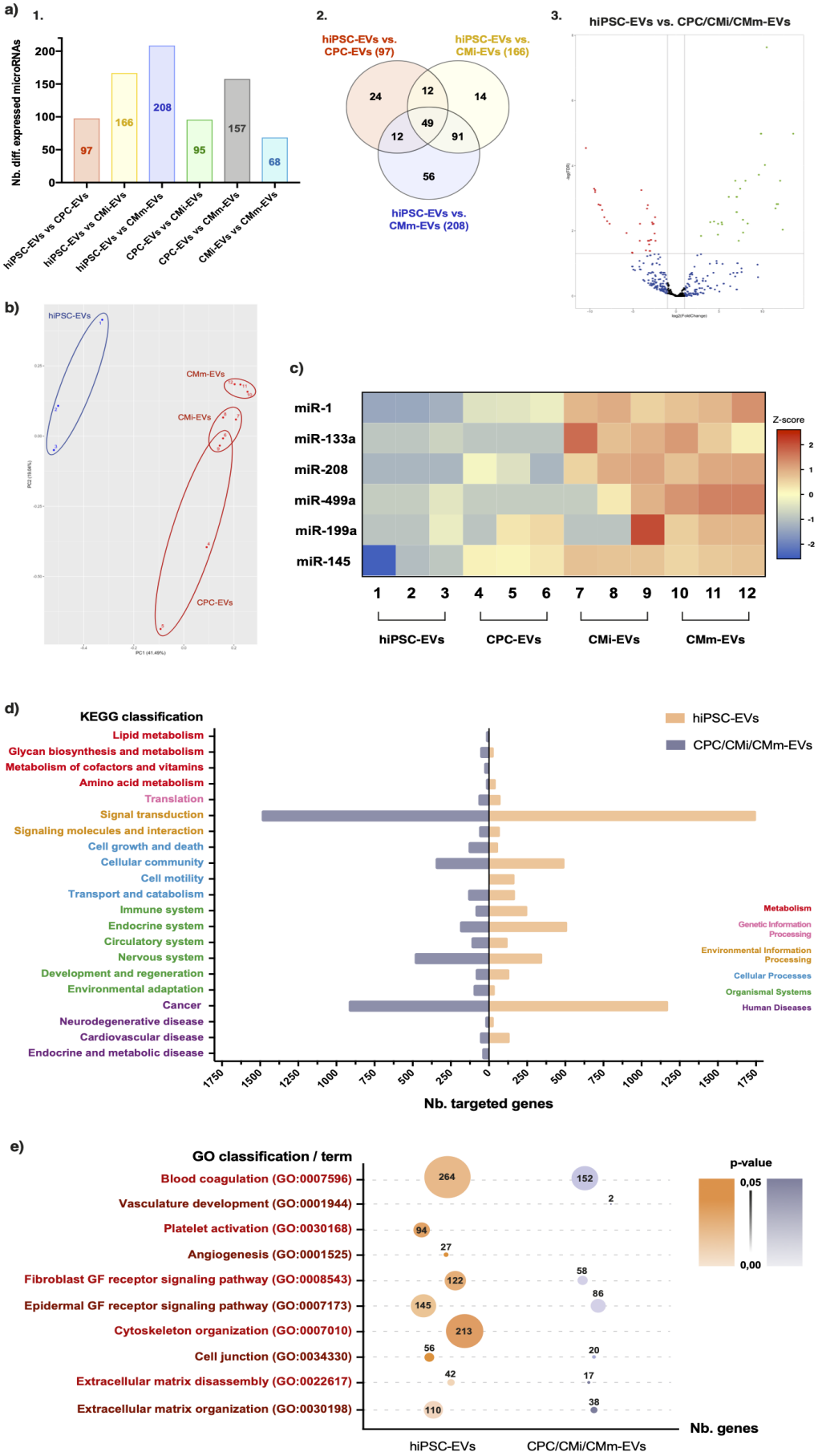
a)
1.
Nb. diff. expressed microRNAs
200
150
100
50
0
97
166
208
95
157
68
hiPSC-EVs vs CPC-EVs
hiPSC-EVs vs CMi-EVs
hiPSC-EVs vs CMm-EVs
CPC-EVs vs CMi-EVs
CPC-EVs vs CMm-EVs
CMi-EVs vs CMm-EVs
2.
hiPSC-EVs vs. CPC-EVs (97)
hiPSC-EVs vs. CMi-EVs (166)
hiPSC-EVs vs. CMm-EVs (208)
24
12
14
12
49
91
56
3.
hiPSC-EVs vs. CPC/CMi/CMm-EVs
b)
hiPSC-EVs
CMm-EVs
CMi-EVs
CPC-EVs
c)
miR-1
miR-133a
miR-208
miR-499a
miR-199a
miR-145
Z-score
2
1
0
-1
-2
1 2 3 4 5 6 7 8 9 10 11 12
hiPSC-EVs
CPC-EVs
CMi-EVs
CMm-EVs
d)
KEGG classification
Lipid metabolism
Glycan biosynthesis and metabolism
Metabolism of cofactors and vitamins
Amino acid metabolism
Translation
Signal transduction
Signaling molecules and interaction
Cell growth and death
Cellular community
Cell motility
Transport and catabolism
Immune system
Endocrine system
Circulatory system
Nervous system
Development and regeneration
Environmental adaptation
Cancer
Neurodegenerative disease
Cardiovascular disease
Endocrine and metabolic disease
hiPSC-EVs
CPC/CMi/CMm-EVs
Metabolism
Genetic Information Processing
Environmental Information Processing
Cellular Processes
Organismal Systems
Human Diseases
1750 1500 1250 1000 750 500 250 0 250 500 750 1000 1250 1500 1750
Nb. targeted genes
e)
GO classification / term
Blood coagulation (GO:0007596)
Vasculature development (GO:0001944)
Platelet activation (GO:0030168)
Angiogenesis (GO:0001525)
Fibroblast GF receptor signaling pathway (GO:0008543)
Epidermal GF receptor signaling pathway (GO:0007173)
Cytoskeleton organization (GO:0007010)
Cell junction (GO:0034330)
Extracellular matrix disassembly (GO:0022617)
Extracellular matrix organization (GO:0030198)
264
152
2
94
27
122
58
145
86
213
56
20
42
17
110
38
p-value
0,05
0,00
Nb. genes
hiPSC-EVs
CPC/CMi/CMm-EVs

Figure 4: Differentially expressed microRNAs in EV samples and respective analysis of KEGG pathways and Gene Ontology biological processes. a) 1. Number of differentially expressed microRNAs (log fold change (FC) $\geq$ 2 or $\leq$ -2 and p-value $\leq$ 0.05.) 1. within EV groups and 2. between hiPSC-EVs and the remaining samples. **3.** Volcano plot displaying statistical significance of microRNA differential expression (DE) between hiPSC-EVs and CPC/CMi/CMm-EVs. Y-axis shows –$\log_{10}$ of the false discovery rate (FDR) and X-axis the $\log_2$FC between groups. Statistical significance increases with Y; Up and down regulated microRNAs in CPC/CMi/CMm-EVs compared to hiPSC-EVs are shown in green and red, respectively. DE data obtained considering CPC, CMi and CMm-EVs samples as replicates of the same group. **b)** Principal Component Analysis (PCA) plot obtained with the 50 microRNAs with highest coefficient of variation (%CV). Cluster groups are plotted against the two highest components of variation (PC1 and PC2). **c)** Heatmap of RNA-Seq expression Z-scores computed for relevant cardiac muscle-miRNAs that are differentially expressed between hiPSC-EVs and CPC/CMi/CMm-EVs groups. **d)** KEGG pathway classification associated with microRNAs upregulated in hiPSC-EVs and CPC/CMi/CMm-EVs. Data shown for each group as the number of targeted genes in each KEGG class. Associated pathways considered significant for p-value $<$ 0.05. **e)** GO classification and term of relevant biological processes associated with microRNAs upregulated in hiPSC-EVs and CPC/CMi/CMm-EVs, presented in a bubble plot. Size of bubbles varies with the number of targeted genes for each biological process, indicated inside or above each bubble; color varies with p-value according to the presented color scale.

could be adopted for this work to increase the angiogenic potential of cardiac-derived EVs, such as exposing the cells to hypoxic conditions prior to CCMed collection. Additionally, enrichment of EVs with specific pro-angiogenic miRNAs could further enhance cardioprotective effects, using miRNAs identified from RNA-seq data analysis.

Lastly, combined bioengineering approaches must be explored to bridge the gap of clinical translation regarding efficient EV delivery and specific cell targeting. Several groups have made progress in this domain through the development of intrinsic and extrinsic strategies (ref.(35)), such as the improvement in biodistribution by means of EV modifications or increase in retention through biomaterial-based platforms for sustained release of EVs.

Materials and Methods

hiPSC culture

The hiPSC line IMR(90)-4 (WiCell) was used for this purpose. hiPSCs were cultured and routinely expanded on Matrigel coated plates (Matrigel hESC-Qualified Matrix, Corning) in serum-free mTeSR™1 medium (StemCell Technologies) at 37°C in a humidified atmosphere of 5% CO_2. The same expansion procedure was followed for hiPSCs to be used for EV isolation (day 0 sample), using feeder-free and animal component-free TeSR-E8™ medium (StemCell Technologies) to ensure complete EV depletion from external sources. Cells tested negative for mycoplasma contamination.

hiPSC differentiation into cardiomyocytes

Differentiation of hiPSCs into CMs was initiated once cells reached 80-90% confluence and was performed following a previously described protocol (36), by temporal modulation of the Wnt/β-catenin signalling. Briefly, at day 0 of differentiation, expansion medium was replaced by RPMI 1640 medium (Thermo Fisher Scientific) supplemented with B27 without insulin (Thermo Fisher Scientific)(RPMI+B27-I), and 80 ng/ml Activin A (PeproTech), 12 μM CHIR99021 (Tocris Bioscience) and 50 μg/ml Ascorbic acid (Sigma-Aldrich). At day 1, approximately 24h after differentiation induction, the medium was replaced by RPMI+B27-I supplemented with 5 μM IWR-1 (Selleckchem) and 50 μg/ml Ascorbic acid (Sigma-Aldrich). At day 3, the medium was replaced by RPMI+B27-I supplemented with 5 μM IWR-1. At day 6, the medium was exchanged for RPMI medium supplemented with B27 with insulin (Thermo Fisher Scientific) (RPMI+B27). Upon reaching 80% of beating cells in monolayer (between days 7 and 8 of differentiation), cells were dissociated by incubation with TrypLE Select (ThermoFisher Scientific) for 8 min and aggregated using AggreWell™400 (STEMCELL Technologies) at a seeding density of 1.500 cell/microwell, according to a previously described protocol (37). Approximately 48h after aggregation, CM aggregates were harvested and transferred to an orbital suspension culture system, at an agitation rate of 90 rpm. Medium (RPMI+B27) was replaced every two days thereafter. At day 15 of culture RPMI+B27 medium was replaced by maturation media, composed of RPMI 1640 without glucose (MP biomedicals, ThermoFisher Scientific) supplemented with B27, 1 mM of glutamine, 10 mM of galactose, 100 μM of oleic acid and 50 μM of palmitic acid, to promote CM metabolic maturation (36). Maturation medium was changed every other day thereafter. CM aggregates were cultured in these conditions for an additional 20 days, reaching a total of 35 days of culture.

HUVEC culture

Human umbilical vein endothelial cells (HUVECs) (catalog No. C2517A, Lonza) were cultured according to the manufacturer's specifications. Briefly, cells were maintained in Endothelial Cell Growth Medium 2 (ECGM-2, Promocell), containing 2% (v/v) of Fetal Calf Serum (FCS, Promocell), in a humidified atmosphere at 37°C in 5% CO_2. Medium was changed every 48h. Cells were subcultured upon reaching 70-85% confluence. HUVECs were only maintained and used for experiments up to passage 5, including.

Conditioned culture medium harvest

Conditioned culture medium (CCMed) was harvested at days 0, 6, 15 and 35 of culture, respectively of hiPSCs, CPCs, immature CMs (CMi) and mature CMs (CMm). For each harvest, total cell number and cell viability were estimated by cell counting using trypan blue exclusion dye. The same volume of medium (180 mL) was collected and processed at each time point.

EV separation from conditioned culture medium

EVs were isolated from CCMed using a combination of differential centrifugation and density gradient ultracentrifugation, which have been shown to outperform other regularly used isolation methods (16; 17). Briefly, the collected CCMed was processed to ensure depletion from major contaminants. For this, two low-speed centrifugation steps (rotor A-4-81, 5810 R centrifuge, Eppendorf) were performed at 4°C immediately after harvest, 1x 300 g for 10 min to remove remaining cells and 1x 2000 g for 10 min to remove apoptotic bodies, followed by a 0.45 μM filtration of the resulting supernatant (Nalgene™ Rapid-Flow™, Thermo Fisher Scientific) to deplete the sample of all other debris. The cleared CCMed was then ultracentrifuged in 30 mL conical open-top polyallomer tubes (Beckman Coulter) at 110.000 g_{max} for 2h45 using a XL-100 ultracentrifuge (SW 28 rotor, Beckman-Coulter) to produce an EV pellet, designated as the 100K pellet. For the density gradient ultracentrifugation, an OptiPrep™ density gradient (ODG, Axis Xield Diagnostics) was prepared as previously described in the literature (16), with minor modifications. An iodixanol working solution (50% (w/v) iodixanol) was made by adding a working solution buffer (60

mM Tris-HCl, 6 mM EDTA, 0.25 M sucrose (pH 7.4)) to a stock solution of OptiPrep™ (60% (w/v) aqueous iodixanol solution). Appropriate amounts of the iodixanol working solution and a homogenization buffer (10 mM Tris-HCl (Tromethamine - Hydrochloric acid), 1 mM EDTA (Ethylenediaminetetraacetic acid) and 0.25 M sucrose (pH 7.4)) were combined in order to prepare 5%, 10%, and 20% (w/v) iodixanol solutions. The 100K pellet was combined with the 50% iodixanol working solution, to create a 40% (w/v) iodixanol EV-containing solution. The discontinuous bottom-up ODG was prepared by loading 4 mL of 40% solution (containing the EV sample) on the bottom of a 16.8 mL open-top polyallomer tube (Beckman Coulter), followed by consecutive layering of 4 mL of 20%, 4 mL of 10%, 3.5 mL of 5% solutions and 1 mL of DPBS. The gradient was centrifuged at 4 °C for 18 h at 110.000 g_{max} using an XL-100 ultracentrifuge (SW 28 rotor, Beckman-Coulter). During centrifugation, EVs migrate upwards by flotation and settle upon reaching their buoyant density. After centrifugation, 16 fractions of 1 mL were collected from top (fraction 1) to bottom (fraction 16). Density fractions 8-9, which have been found to contain most of the EV sample of interest (16), were pooled and concentrated to 300 µL using Amicon Ultra-2 mL 10 KDa filter units (Merck Millipore). Negative and positive control gradients were prepared with blank DPBS and Fetal Bovine Serum (FBS qualified, EU-approved, Gibco, Thermo Fisher Scientific), respectively.

Nanoparticle Tracking Analysis

Nanoparticle tracking analysis (NTA) was performed using the NanoSight NS300 (Malvern Instruments Ltd., Malvern, UK) equipment, with a 488 nm laser ($<$ 55 mW maximum power) and an automatic syringe pump system. NTA was used to measure size, size distribution and concentration of particles from the pooled Optiprep™ density gradient EV-rich fractions 8-9. Three videos of 60 s were recorded for each individual sample and considered using detection threshold 3, camera level 14 and a syringe pump infusion speed of 40. All videos were analysed by NTA software version 3.3. To achieve optimal measurements, samples were diluted with DPBS to obtain a particle concentration within the ideal range for the NTA software (3.10^8 – 1.10^9 particles/mL). All size distributions determined with NTA correspond to the hydrodynamic diameters of the particles in suspension, as estimated by the Stokes-Einstein equation.

Transmission Electron Microscopy

Transmission Electron Miscroscopy (TEM) was performed on EV-rich fractions 8-9. A drop (5 µL) of sample was deposited on a precoated formvar/carbon 150 mesh Veco copper grid for 2 min. Grids were fixed with 4% (w/v) PFA for 20 min, washed with sterile water, stained with 2% (w/v) uranyl acetate for 2 min and dried at room temperature (20-22°C). Grids were examined using electron microscopy (Hitachi H-7650, 120 KV electron microscope, Hitachi High-Technologies Corporation).

Western Blotting

Western blot was performed on EV-rich fractions 8-9 and whole cell lysates for EV specific transmembrane protein CD63 and cytosolic protein Flotillin-2 (38), and for non-EV common contaminant AGO2 (21). EV samples were normalized by volume (20 µL of sample per lane) and whole cell lysates were normalized by protein amount (10 µg of protein was applied per lane). Protein concentrations were determined by BCA (ThermoFisher Scientific). Samples were diluted in lysis buffer (NuPAGE LDS sample buffer 4x, Novex, Life Technologies Europe B.V.) in reducing (Flotillin-2, AGO2) or non-reducing conditions (CD63) and boiled for 5 min at 95°C. Protein samples were separated by SDS polyacrylamide gel electrophoresis in MES running buffer (Novex, Life Technologies Europe B.V.) for 50 min and transferred to a nitrocellulose membrane (iBlot Transfer Stack, nitrocellulose, mini, Novex, Life Technologies Europe B.V.). Membranes were stained with Ponceau S solution (Sigma Aldrich) immediately after transfer for acquisition of pictures to confirm the success of the transfer, and then washed with distilled water, de-stained with 1 M NaOH solution, and again washed extensively with distilled water. Membranes were blocked with 5% (w/v) skim milk in Tris-Buffered Saline + 0.1% (v/v) Tween 20 (TBST) for 1h at room temperature and then incubated overnight at 4°C in primary antibodies diluted in 5% skim milk prepared in TBST: CD63 (1:1.000, ab59479, Abcam), Flotillin-2 (1:1.000, 610383, BD) and AGO2 (1:1.000, ab32381, Abcam). The following day, membranes were washed with TBST, incubated with the respective secondary antibody for 1h at room temperature (anti-rabbit HRP, 1:20.000, System Biosciences; anti-mouse ECL, 1:5.000/ 1:10.000, NA931V, GE Lifesciences) and then washed again. For the revelation step, chemiluminescent substrate (WesternBright Sirius, Advansta) was added to the membranes according to the manufacturer's instructions and imaging was performed using a ChemiDoc imaging system (Bio-Rad Laboratories, Hercules).

EV labelling with PKH26 and uptake assays

EV labelling was performed using the PKH26 Red Fluorescent Cell Linker Mini Kit for General Cell Membrane Labelling (Sigma-Aldrich) according to the manufacturer's instructions. A negative control was prepared with PBS following the same protocol. Stained vesicles (PKH26-EVs) and the corresponding control (PKH26-PBS) were loaded on the bottom of a density gradient, and ultracentrifuged as previously described, to separate labelled particles from unbound dye. HUVECs were seeded in 8-well chamber Ibidi slides (Ibidi GmH) at a density of 8.000 cells/cm^2 or in 12-well plates at a density of 18.000 cells/cm^2, to be used for immunofluorescence and flow cytometry respectively. Cells were treated with PKH26-EVs or PKH26-PBS appropriately diluted in ECGM-2, at a dose of 3.000 particles per cell. For each sample, 1 well was prepared with the addition of dynamin inhibitor Dynasore (Sigma Aldrich) in a concentration of 50 µM, to prevent EV uptake. HUVECs were incubated for 2h30 in a humidified environment (37 °C, 5% CO_2). Cells to be used for flow cytometry were washed twice with FACS buffer and then analysed using a BD FACS Celesta™ cytometer (BD Biosciences). Cells to be used for immunofluorescence were fixed with 4% PFA (w/v) for 20 min at room temperature, and then stained for CD31 marker. For this, fixed cells were washed twice with DPBS, blocked with 0.2% (w/v) FSG for 30 min at room temperature and incubated overnight with primary anti-CD31 antibody diluted in 0.2% FSG (1:50; clone JCF0A, M0823, DAKO Omnis, Agilent Technologies), or the corresponding mouse IgG isotype control (1:50, sc-3877, Santa Cruz Biotechnology) at 4°C. The following day, cells were washed with DPBS and incubated with secondary antibody diluted in 0.2% FSG (1:200, Alexa 647, donkey anti-mouse IgG, 31571, ThermoFisher Scientific) for 1h at room temperature. Nuclei were counterstained with DAPI (ThermoFisher Scientific) in DPBS. Fluorescence images were acquired using an inverted fluorescence microscope (DMI6000, Leica Microsystems GmbH) and signal intensity was quantified using ImageJ software.

Wound healing assay

HUVECs were seeded at 35.000 cells per well onto 48-well plates coated with 0.1% (w/v) gelatin (Sigma-Aldrich). A sterile 200 µL pipette tip was used to create a scratch in the cell monolayer, after which cells were washed twice with DPBS. EV samples were diluted in appropriate amounts of reduced-supplementation media (with 0.5% (v/v) FCS and without growth factors) and blank gradient. Positive (fully supplemented ECGM-2), untreated negative (Endothelial Cell Basal Medium-2 (ECBM-2, consisting of ECGM-2 without any added supplements) + 0.5% FCS) and FBS-EVs (isolated through the same process as CCMed) controls were prepared. Vehicle controls, consisting of the 8-9 fractions of a blank gradient in volumes consistent with each EV sample, were also prepared for each day 0, 6, 15 and 35. The same procedure was conducted with the addition of Dynasore in concentration of 50 µM (Sigma-Aldrich), which inhibits the uptake of EVs by HUVECs and

demonstrates that the wound healing effect observed in the assay is indeed mediated by EVs. 500 µL of corresponding treatment was added per well, normalized to a dose of 3.000 particles per cell. Cells were placed in a humidified environment (37 °C, 5% CO_2) and images were acquired at time-points 0h, 8h and 24h post-scratch using an inverted microscope (DMI6000, Leica Microsystems GmbH). Wound width was analysed with MRI Wound Healing tool of ImageJ software, by calculating the percentage of wound closure relative to time-point 0h.

Tube formation assay

HUVECs were seeded at 12.000 cells per well onto 48-well plates coated with 40 µL of basement membrane extract (Matrigel Growth Factor Reduced (GFR) Basement Membrane Matrix, Phenol Red-Free, Corning). HUVECs were resuspended in the corresponding EV sample appropriately diluted in ECBM-2, at a dose of 3.000 particles per cell. Positive (ECGM-2), untreated negative (ECBM-2), FBS, PBS and vehicle controls were prepared. For each sample, the same procedure was conducted with the addition of Dynasore in concentration of 50 µM. To validate the efficacy of this assay, Suramin Sodium Salt (TargetMol), an inhibitor of endothelial cell proliferation and migration, was added to positive control cells in concentrations of 5 µM and 10 µM diluted in ECGM-2. The plate was placed in a humidified environment (37 °C, 5% CO_2) for 8 h. Cells were then stained with a 1:500 solution of FDA (Sigma-Aldrich) in DPBS. Fluorescence images were acquired at 5x magnification using an inverted fluorescence microscope (DMI6000, Leica Microsystems GmbH). Pictures were analysed using the Angiogenesis Analyzer plugin of ImageJ software.

MicroRNA analysis

Total RNA was isolated from EV samples (N=3 replicates for each sample) using Norgen Biotek Exosomal RNA Isolation Kit (Cat.58000). microRNA library preparation was performed by PCR amplification using Norgen Biotek Small RNA Library Prep Kit (Cat. 63600) and library quality control was achieved using Bioanalyzer to estimate library size and concentration. Libraries were denatured and diluted to the required concentration and then applied onto the suitable flowcell and sequenced using Illumina NextSeq 500 sequencing platforms. Data analysis was carried out using an advanced pipeline for processing of raw reads and mapping to the genome and annotated transcriptome. Data was filtered and normalized using the trimmed mean of M-values (TMM) normalization method for differential expression (DE) analysis. DE analysis between each two groups was performed using the EdgeR statistical software package and false discovery rate was adjusted through the Benjamini-Hochberg procedure. For the comparison of hiPSC-EVs with the designated CPC/CMi/CMm-EVs group, replicates of each biological group were considered as individual replicates of the CPC/CMi/CMm-EVs group. DE was considered significant for log fold change ≥ 1 or ≤ -1 at p-value and FDR ≤ 0.05. Results were further trimmed by considering only miRNAs with log fold change ≥ 2 or ≤ -2. Putative targets of up- and down-regulated miRNAs between hiPSC-EVs and CPC/CMi/CMm-EVs were predicted, along with KEGG pathways and GO-terms analysis from the selected targets, using the DIANA-miRPath v3 software, considering only results with p-value ≤ 0.05.

Statistical analysis

Statistical analysis was entirely performed using GraphPad Prism 7 (GraphPad Software). Significance was tested using either Student's T test or one-way ANOVA. Statistical significance was considered for p-values < 0.05. All experimental outcomes correspond to a minimum of 3 biological replicates, with the exception of CMm-EVs, with 2 biological replicates and technical duplicates for one of the replicates.

References

[1] Benjamin, E. J., Muntner, P., Alonso, A. et al. (2019). Heart disease and stroke statistics-2019 update: a report from the American Heart Association, Circulation, 139(10), 56–528. doi:10.1161/CIR.0000000000000659.

[2] Madonna, R., Van Laake, L. W., Davidson, S. M., Engel, F. B., Hausenloy, D. J., Lecour, S., ... Sluijter, J. P. G. (2016). Position Paper of the European Society of Cardiology Working Group Cellular Biology of the Heart: cell-based therapies for myocardial repair and regeneration in ischemic heart disease and heart failure. European Heart Journal, 37(23), 1789–1798. doi:10.1093/eurheartj/ehw113

[3] Waldenström, A., Gennebäck, N., Hellman, U. & Ronquist, G. (2012). Cardiomyocyte Microvesicles Contain DNA/RNA and Convey Biological Messages to Target Cells. PLoS ONE, 7(4), e34653. doi:10.1371/journal.pone.0034653

[4] Sluijter, J. P. G., Davidson, S. M., Boulanger, C. M., Buzás, E. I., de Kleijn, D. P. V., Engel, F. B., ... Ferdinandy, P. (2017). Extracellular vesicles in diagnostics and therapy of the ischaemic heart: Position Paper from the Working Group on Cellular Biology of the Heart of the European Society of Cardiology. Cardiovascular Research, 114(1), 19–34. doi:10.1093/cvr/cvx211

[5] Colombo, M., Raposo, G., & Théry, C. (2014). Biogenesis, Secretion, and Intercellular Interactions of Exosomes and Other Extracellular Vesicles. Annual Review of Cell and Developmental Biology, 30(1), 255–289. doi:10.1146/annurev-cellbio-101512-122326

[6] Minciacchi V. R., You S., Spinelli C., Morley S., Zandian M., Aspuria P., Cavallini L., Ciardiello C., Sobreiro M., Morello M., Kharmate G., Jang S. Chul & Kim D. (2015). Large oncosomes contain distinct protein cargo and represent a separate functional class of tumor-derived extracellular vesicles. Oncotarget, 6(13), 11327-11341. doi:10.18632/oncotarget.3598

[7] Van Niel, G., D'Angelo, G. & Raposo, G. (2018). Shedding light on the cell biology of extracellular vesicles. Nature Reviews Molecular Cell Biology, 19(4), 213–228. doi:10.1038/nrm.2017.125

[8] Adamiak, M., Cheng, G., Bobis-Wozowicz, S., Zhao, L., Kedracka-Krok, S., Samanta, A., ... Zuba-Surma, E. K. (2017). Induced Pluripotent Stem Cell (iPSC)–Derived Extracellular Vesicles Are Safer and More Effective for Cardiac Repair Than iPSCs. Circulation Research, 122(2), 296–309. doi:10.1161/circresaha.117.311769

[9] Colao, I. L., Corteling, R., Bracewell, D., & Wall, I. (2018). Manufacturing Exosomes: A Promising Therapeutic Platform. Trends in Molecular Medicine, 24(3), 242–256. doi:10.1016/j.molmed.2018.01.006

[10] Harane, N. E., Correa, B. L., Gomez, I., Hocine, H. R., Vilar, J., Desgres, M., ... Silvestre, J.-S. (2020). Extracellular Vesicles from Human Cardiovascular Progenitors Trigger a Reparative Immune Response in Infarcted Hearts. Cardiovascular Research. doi:10.1093/cvr/cvaa028

[11] Zhang, Z., Yang, J., Yan, W., Li, Y., Shen, Z., & Asahara, T. (2016). Pretreatment of Cardiac Stem Cells With Exosomes Derived From Mesenchymal Stem Cells Enhances Myocardial Repair. Journal of the American Heart Association, 5(1), e002856. doi:10.1161/jaha.115.002856

[12] Barile, L., Lionetti, V., Cervio, E., Matteucci, M., Gherghiceanu, M., Popescu, L. M. & Vassalli, G. (2014). Extracellular vesicles from human cardiac progenitor cells inhibit cardiomyocyte apoptosis and improve cardiac function after myocardial infarction. Cardiovascular Research, 103(4), 530–541. doi:10.1093/cvr/cvu167

[13] Barile, L., Cervio, E., Lionetti, V., Milano, G., Ciullo, A., Biemmi, V., ... Vassalli, G. (2018). Cardioprotection by cardiac progenitor cell-secreted exosomes: role of pregnancy-associated plasma protein-A. Cardiovascular Re-

search, 114(7), 992–1005. doi:10.1093/cvr/cvy055

[14] Ribeiro-Rodrigues, T. M., Laundos, T. L., Pereira-Carvalho, R., Batista-Almeida, D., Pereira, R., Coelho-Santos, V., Silva, A. P., Fernandes, R., Zuzarte, M., Enguita, F. J., Costa, M. C., Pinto-do-Ó, P., Pinto, M. T., Gouveia, P., Ferreira, L., Mason, J. C., Pereira, P., Kwak, B. R., Nascimento, D. S., & Girão, H. (2017). Exosomes secreted by cardiomyocytes subjected to ischaemia promote cardiac angiogenesis. Cardiovascular research, 113(11), 1338–1350. doi:10.1093/cvr/cvx118

[15] Patel, G. K., Khan, M. A., Zubair, H., Srivastava, S. K., Khushman, M., Singh, S., & Singh, A. P. (2019). Comparative analysis of exosome isolation methods using culture supernatant for optimum yield, purity and downstream applications. Scientific Reports, 9(1). doi:10.1038/s41598-019-41800-2

[16] Van Deun, J., Mestdagh, P., Sormunen, R., Cocquyt, V., Vermaelen, K., Vandesompele, J. & Hendrix, A. (2014). The impact of disparate isolation methods for extracellular vesicles on downstream RNA profiling. Journal of Extracellular Vesicles, 3(1), 24858. doi:10.3402/jev.v3.24858

[17] Kalra, H., Adda, C. G., Liem, M., Ang, C.-S., Mechler, A., Simpson, R. J. & Mathivanan, S. (2013). Comparative proteomics evaluation of plasma exosome isolation techniques and assessment of the stability of exosomes in normal human blood plasma. PROTEOMICS, 13(22), 3354–3364. doi:10.1002/pmic.201300282

[18] Lobb, R. J., Becker, M., Wen Wen, S., Wong, C. S. F., Wiegmans, A. P., Leimgruber, A., & Möller, A. (2015). Optimized exosome isolation protocol for cell culture supernatant and human plasma. Journal of Extracellular Vesicles, 4(1), 27031. doi:10.3402/jev.v4.27031

[19] El Harane, N., Kervadec, A., Bellamy, V., Pidial, L., Neametalla, H. J., Perier, M.-C. & Renault, N. K. E. (2018). Acellular therapeutic approach for heart failure: in vitro production of extracellular vesicles from human cardiovascular progenitors. European Heart Journal, 39(20), 1835–1847. doi:10.1093/eurheartj/ehy012

[20] Brennan, K., Martin, K., FitzGerald, S. P., O'Sullivan, J., Wu, Y., Blanco, A., ... Mc Gee, M. M. (2020). A comparison of methods for the isolation and separation of extracellular vesicles from protein and lipid particles in human serum. Scientific Reports, 10(1). doi:10.1038/s41598-020-57497-7

[21] Lötvall, J., Hill, A. F., Hochberg, F., Buzás, E. I., Di Vizio, D., Gardiner, C., Gho, Y. S., Kurochkin, I. V., Mathivanan, S., ... Théry, C. (2014). Minimal experimental requirements for definition of extracellular vesicles and their functions: a position statement from the International Society for Extracellular Vesicles. Journal of extracellular vesicles, 3, 26913. doi:10.3402/jev.v3.26913

[22] Patan S. (2000). Vasculogenesis and angiogenesis as mechanisms of vascular network formation, growth and remodeling. Journal of neuro-oncology, 50(1-2), 1–15. doi:10.1023/a:1006493130855

[23] Vrijsen, K. R., Sluijter, J. P., Schuchardt, M. W., van Balkom, B. W., Noort, W. A., Chamuleau, S. A., & Doevendans, P. A. (2010). Cardiomyocyte progenitor cell-derived exosomes stimulate migration of endothelial cells. Journal of cellular and molecular medicine, 14(5), 1064–1070. doi:10.1111/j.1582-4934.2010.01081.x

[24] Dougherty, J. A., Kumar, N., Noor, M., Angelos, M. G., Khan, M., Chen, C. A., & Khan, M. (2018). Extracellular Vesicles Released by Human Induced-Pluripotent Stem Cell-Derived Cardiomyocytes Promote Angiogenesis. Frontiers in physiology, 9, 1794. doi:10.3389/fphys.2018.01794

[25] Ding, Q., Sun, R., Wang, P., Zhang, H., Xiang, M., Meng, D., ... Chen, S. (2018). Protective effects of human induced pluripotent stem cell-derived exosomes on high glucose-induced injury in human endothelial cells. Experimental and Therapeutic Medicine. doi:10.3892/etm.2018.6059

[26] Liu, B., Lee, B. W., Nakanishi, K., Villasante, A., Williamson, R., Metz, J., ... Vunjak-Novakovic, G. (2018). Cardiac recovery via extended cell-free delivery of extracellular vesicles secreted by cardiomyocytes derived from induced pluripotent stem cells. Nature Biomedical Engineering, 2(5), 293–303. doi:10.1038/s41551-018-0229-7

[27] Del Fattore, A., Luciano, R., Saracino, R., Battafarano, G., Rizzo, C., Pascucci, L. & Muraca, M. (2014). Differential effects of extracellular vesicles secreted by mesenchymal stem cells from different sources on glioblastoma cells. Expert Opinion on Biological Therapy, 15(4), 495–504. doi:10.1517/14712598.2015.997706

[28] Thum, T., Catalucci, D., & Bauersachs, J. (2008). MicroRNAs: novel regulators in cardiac development and disease. Cardiovascular Research, 79(4), 562–570. doi:10.1093/cvr/cvn137

[29] Sluijter, J. P. G., van Mil, A., van Vliet, P., Metz, C. H. G., Liu, J., Doevendans, P. A., & Goumans, M. J. (2010). MicroRNA-1 and -499 Regulate Differentiation and Proliferation in Human-Derived Cardiomyocyte Progenitor Cells. Arteriosclerosis, Thrombosis, and Vascular Biology, 30(4), 859–868. doi:10.1161/atvbaha.109.197434

[30] Bayless, K. J., & Johnson, G. A. (2011). Role of the Cytoskeleton in Formation and Maintenance of Angiogenic Sprouts. Journal of Vascular Research, 48(5), 369–385. doi:10.1159/000324751

[31] Brill, A., Elinav, H., & Varon, D. (2004). Differential role of platelet granular mediators in angiogenesis. Cardiovascular Research, 63(2), 226–235. doi:10.1016/j.cardiores.2004.04.012

[32] Murakami, M., Nguyen, L. T., Zhuang, Z. W., Moodie, K. L., Carmeliet, P., Stan, R. V., & Simons, M. (2008). The FGF system has a key role in regulating vascular integrity. The Journal of clinical investigation, 118(10), 3355–3366. https://doi.org/10.1172/JCI35298

[33] Borosch, S., Dahmen, E., Beckers, C., Stoppe, C., Buhl, E. M., Denecke, B., ... Kraemer, S. (2017). Characterization of extracellular vesicles derived from cardiac cells in an in vitro model of preconditioning. Journal of Extracellular Vesicles, 6(1), 1390391. doi:10.1080/20013078.2017.1390391

[34] Garcia, N. A., Ontoria-Oviedo, I., González-King, H., Diez-Juan, A., & Sepúlveda, P. (2015). Glucose Starvation in Cardiomyocytes Enhances Exosome Secretion and Promotes Angiogenesis in Endothelial Cells. PLOS ONE, 10(9), e0138849. doi:10.1371/journal.pone.0138849

[35] de Abreu, R. C., Fernandes, H., da Costa Martins, P. A., Sahoo, S., Emanueli, C., & Ferreira, L. (2020). Native and bioengineered extracellular vesicles for cardiovascular therapeutics. Nature reviews. Cardiology, 17(11), 685–697. doi:10.1038/s41569-020-0389-5

[36] Correia, C., Koshkin, A., Duarte, P., Hu, D., Teixeira, A., Domian, I., Serra, M. & Alves, P. M. (2017). Distinct carbon sources affect structural and functional maturation of cardiomyocytes derived from human pluripotent stem cells. Scientific Reports, 7(1). doi:10.1038/s41598-017-08713-4

[37] Correia, C., Koshkin, A., Duarte, P., Hu, D., Carido, M., Sebastião, M. J., Gomes-Alves, P., Elliott, D. A., Domian, I. J., Teixeira, A. P., Alves, P. M. & Serra, M. (2018). 3D aggregate culture improves metabolic maturation of human pluripotent stem cell derived cardiomyocytes. Biotechnology and bioengineering, 115(3), 630–644. doi:10.1002/bit.26504

[38] Théry, C., Witwer, K. W., Aikawa, E., Alcaraz, M. J., Anderson, J. D., Andriantsitohaina, R., Atkin-Smith, ... G. K. (2018). Minimal information for studies of extracellular vesicles 2018 (MISEV2018): a position statement of the International Society for Extracellular Vesicles and update of the MISEV2014 guidelines. Journal of Extracellular Vesicles, 8(1), 1535750. doi:10.1080/20013078.2018.1535750